IAC-18.B1.5.4x44474

Navigation Assistance in Polar Waters through Information on Sea Ice Drift and Coverage Derived from Spaceborne Synthetic Aperture Radar Images

Anja Frost [a]*, Maurice Wiercioch[a], Suman Singha[a], Andrey Pleskachevsky[a], Stefan Wiehle[a], Sven Jacobsen[a]

[a] *DLR (German Aerospace Center), Maritime Safety and Security Lab Bremen, Henrich-Focke-Str. 4, 28199 Bremen,* anja.frost@dlr.de
* Corresponding Author

Abstract

In polar waters, ship routes can become impassable within hours because of drifting sea ice. In this paper, we present a new software processor that is designed to derive high resolution sea ice drift fields from spaceborne Synthetic Aperture Radar images along with information on local sea ice coverage. The determination of local sea ice coverage is based on polarimetric features gained from the radar image data. The core of the subsequent sea ice drift estimation is the well-known phase correlation technique, executed within a hierarchical motion estimation framework. The output is a vector field indicating the sea ice motion. We tested the proposed software processor with images provided by the satellites TerraSAR-X and RADARSAT-2, acquired during a field campaign in the Southern Ocean in January 2017. Derived sea ice drift fields show converging and diverging ice sheets, and sheering zones. Most open water areas are identified successfully by prior sea ice coverage determination. The drift vector field, delivered to the bridge of polar operating ships in near real-time, can improve navigation in ice-infested waters.
Keywords: Sea ice motion, sea ice classification, polarimetry, correlation, near real-time, fusion

Acronyms/Abbreviations

Deutsches Zentrum für Luft- und Raumfahrt (DLR)
Synthetic Aperture Radar (SAR)
TerraSAR-X (TS-X)
RADARSAT-2 (RS-2)
Near real-time (NRT)

1. Introduction

Ship navigation in polar waters is challenging. Extreme wind speeds and temperatures, the presence of sea ice and icebergs, and the remoteness of the region make high demands on humans and technology. In addition, sea ice is subject of constant changes. Winds and ocean currents can shove sea ice floes together over kilometers, and close well navigable open water leads within hours. When the pressure process continues, sea ice floes are piled up one over another, or are forced upright into a wall called pressure ridge [1]. Such obstacles are hard to cross, even for icebreakers. Hence, up-to-date information on the current conditions of sea ice is requested to ensure safe ship operation [2].

Synthetic Aperture Radar (SAR) satellites such as Canada's RADARSAT-2 (RS-2) or Germany's TerraSAR-X (TS-X) are well suited to observe polar waters. Due to their active radar antenna, they make visible the boundaries of sea ice and different structures within the ice, independently of cloud cover. As they are operating in a sun-synchronous orbit, they pass the poles multiple times per day, which allows us to monitor a selected location in high latitudes frequently. Exemplarily, Table 1 lists the revisit time of TS-X over selected arctic and antarctic locations. In turn, frequent acquisitions allow the mapping of small-scale changes in sea ice.

In this paper, we present a new software processor that is intended to retrieve high resolution sea ice drift fields from pairs of sequential, co-located TS-X and RS-2 images. The derived sea ice drift fields reveal spatial changes in ice velocity and direction and thus can be used to identify the location and extend of converging or diverging ice zones, pressure ridges and to border ice sheets that show individual motion.

The estimation of sea ice drift fields is based on the well-known phase correlation technique [3] that automatically recognizes recurring sea ice patterns in the SAR image pairs. Phase correlation technique is widely-used in image registration in general and sea ice motion tracking in particular [4][5][6], but it fails if there are no unique structures (i.e. patterns) in the image data. This is the case

* in open water and low sea ice concentration
* in very smooth or homogeneous sea ice
* if sea ice has undergone strong deformations

so that patterns can no more be recognized [7]. In order to address at least the first source for failures, we now added sea ice coverage mapping prior to drift estimation, utilizing a Neural Network fed with polarimetric features [8]. Sea ice drift estimation is then carried out in sea ice covered areas only.

First tests on the drift estimation algorithm (without prior sea ice coverage mapping) we carried out with campaign data collected in 2016/2017 during Antarctic

Table 1. Revisit time of TerraSAR-X over exemplarily arctic and antarctic locations

	Lat	Lon	Acquisitions* in 11 days
Cape Denison, Antarctica	-67.00°	142.67°	7
Cape Farewell, Greenland	59.77°	-43.91°	5
Lancaster Sound, Northwest Passage	74.14°	80.84°	9
Vilkitsky Strait, Northeast Passage	77.97°	104.13°	12
Hans Island, Nares Strait	80.83°	-66.45°	17

* only acquisitions with incidence angle range from 20° to 45° and right looking configuration are taken into account. Please mind that it is possible to enlarge the incidence angle range and also choose left looking configuration, which nearly doubles the number of possible acquisitions. But increasing the incidence angle range causes lower image quality, and the switching of the antenna looking direction is accompanied by time and energy loss.

Circumnavigation Expedition [9], and presented our results in [10]. Now, we use an image pair from the same campaign to demonstrate the improvement gained by adding sea ice coverage mapping.

2. TerraSAR-X and RADARSAT-2

In this work, we use image data provided by the satellites TS-X and RS-2. Both satellites are equipped with a solar array for energy supply and therefore operate in a sun synchronous orbit.

TS-X circulates the earth at 514 m altitude and with a nominal revisit period of 11 days (167 orbits within revisit period, 15 2/11 orbits per day). It has left and right side observation capability. The right side looking radar is preferred because of power constraints in the left side configuration; the solar array is no more pointing into the sun. In addition, the communications link to the ground is obstructed. [11]

RS-2 operates at 798 km altitude with 14 7/34 orbits per day. It also has left- and right-looking radar orientation capability. [12]

Combining TS-X and RS-2 satellites makes it possible to considerably shorten the time difference between two acquisitions taken over a selected region.

3. Processing chain

The proposed software processor reads in pairs of SAR intensity images. Both images are calibrated to sigma naught. The older image is geometrically co-registered to the newer image. Also, sea ice covered areas are differentiated from open water, generating a binary map. Subsequently, sea ice drift estimation is outperformed in identified sea ice covered areas only.

Figure 1 illustrates the main processing steps of the processor. Please note that the sea ice coverage extraction involves all polarimetric channels, while sea ice drift estimation is carried out on HH channel only.

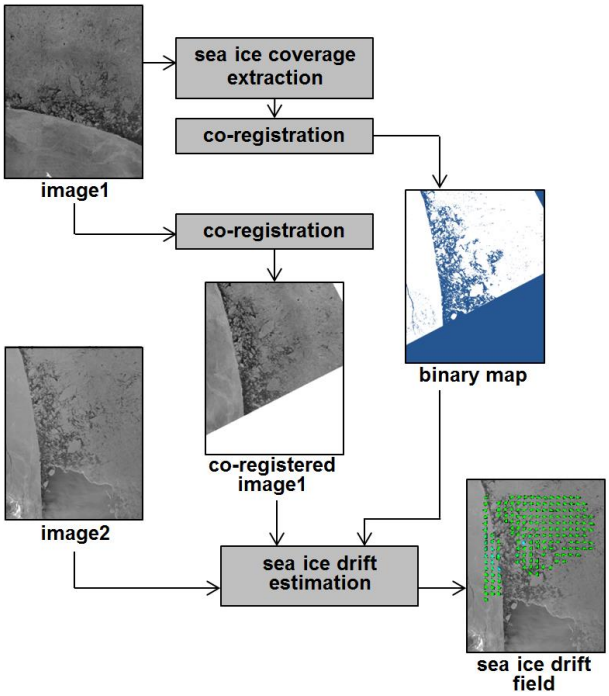

Fig.1. Main processing steps

3.1 Sea ice coverage

In SAR data, open water and sea ice show different characteristics. The backscatter response of open water is comparatively low, though it increases at higher wind speeds [13]. In addition, the imaged sea surface is usually more homogeneous then sea ice covered areas. Even at high sea state, wave crests occur in regular patterns [14] and can be identified by pattern recognition techniques. The different characteristics of open water and sea ice forms the basis for automated sea ice coverage extraction.

In our work, we utilize our sea ice type classification algorithm [8][15][16] that generates polarimetric features from dual-pol SAR data. Then, the features are fed into a trained artificial neural network, which classifies each pixel. The result is a binary map indicating open water areas.

The binary map is handed over to the sea ice drift estimation module of our processor.

3.2 Sea ice drift

For sea ice drift estimation from pairs of co-located and co-registered SAR images, we apply the phase correlation method [3] that is based on a frequency-domain representation of the SAR data calculated by fast Fourier transform.

The fast Fourier transform is outperformed in sliding windows the size of $N \times N$ pixel, i.e. in squared image patches

$$g(i, j) = \text{image1}(x+i, y+j) * \text{w}(i, j) \quad (1)$$
$$h(i, j) = \text{image2}(x+i+u_k, y+j+v_k)) * \text{w}(i, j) \quad (2)$$

with i=0…N-1, j=0…N-1 (see Fig. 2). (u_k, v_k) represents the drift vector to be estimated iteratively within a hierarchical motion estimation framework. k indicates the iteration number. In the first iteration, we initialize u_1=0 and v_1=0.

w(i, j) denotes a discrete window function that is used in order to avoid discontinuities at the patch margins. In our work, we apply the Hann function [10]:

$$w(n) = \frac{1}{2}\left(1 - cos\frac{2\pi n}{N-1}\right) \quad (3)$$

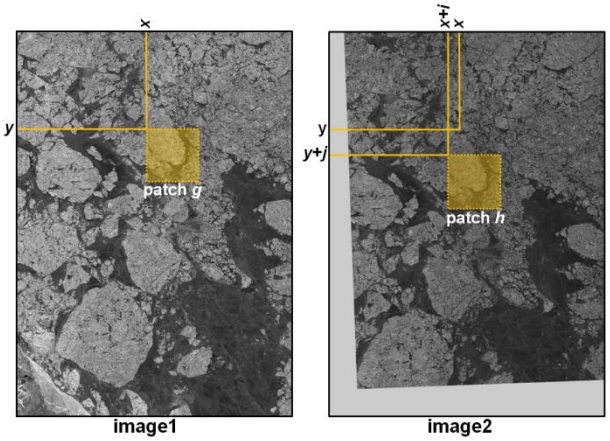

Fig.2. Principle of drift estimation from squared image patches extracted from two sequential SAR images

From the Fourier-transformed image patches $\mathfrak{F}(g)$ and $\mathfrak{F}(h)$, we calculate the normalized image cross spectrum

$$PC(i,j) = \mathfrak{F}^{-1}\left(\frac{\mathfrak{F}(g)\cdot\mathfrak{F}^*(h)}{|\mathfrak{F}(g)\cdot\mathfrak{F}^*(h)|}\right) \quad (4)$$

that shows a peak indicating the shift of the pattern visible in both image patches:

$$(\Delta u, \Delta v) = \arg\max PC(i,j) \quad (5)$$

The drift vector is updated, i.e. (u_{k+1}, v_{k+1}) = (u_k+Δu, v_k+Δv). The procedure is repeated with a newly extracted image patch h until optimal pattern match is found with Δu=0 and Δv=0.

In addition to the iterative update of a drift vector (u_k, v_k), we execute the estimation within a multi-resolution Gaussian image pyramid consisting in 4 resolution layers with a reduction factor of 2. The estimation starts in the coarsest resolution, and step by step processes higher resolution layers. The size of the patches is kept constant at *128 × 128* pixels. Hence, the coverage in square kilometre is high at the coarsest resolution and halved with each higher resolution layer.

The hierarchical processing compromises between large-scale image patches which may contain varying ice motion and small-scale image patches which do not capture large sea ice displacements.

A more detailed description of the drift estimation is given in our previous work [10]. The hierarchical concept is explained in [6].

4. Results and discussion

Our test deals with an image pair acquired over the Southern Ocean, close to Cape Denison (67.00°S, 142.67°E). Footprints of the images are given in Figure 3. Further details on the acquisitions are listed in Table 2.

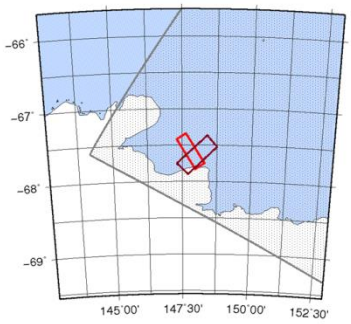

Fig.3. Footprints of a TS-X image (red) taken on 2017/01/30 at 10:09 UTC and a RS-2 image (dark red) taken on 2017/01/30 at 10:36 UTC.

Figure 4 shows the TS-X intensity image co-registered to the following RS-2 acquisition (Figure 5). The scene includes several very large icebergs surrounded by sea ice and open water.

Sea ice drift vectors estimated without sea ice coverage extraction are superimposed in Figure 5. 8 % of the drift vectors can be manually identified as erroneous. The errors result from the homogeneous surface of open water and from sea ice deformation close the left margin of the TS-X image.

Figure 7 shows the sea ice drift field generated with our proposed software processor, i.e. including the sea ice coverage map (depict in Figure 6). As can be seen, most of the erroneous drift vectors in the open water area are successfully filtered out. The amount of insufficient drift vectors is reduced to 1.5 %. In the area of manually determined open water, 88 % of the formerly erroneous drift vectors are eliminated. The remaining drift vectors in the open water area are caused by noise in the sea ice coverage map. A smoothing of the coverage map effects a further reduction of insufficient drift vectors.

In the sea ice covered area, we lose 0.4 % of correct drift vectors in consequence of wrong sea ice coverage mapping.

5. Conclusions

The reliability of a phase-correlation based estimator for sea ice drift fields from pairs of co-located, sequential SAR images depends on the presence of significant structures i.e. patterns in the images. The estimation fails in case of open water and low sea ice concentration. In order to eliminate erroneous drift vectors, we added a new sea ice coverage extraction module to our sea ice drift estimation processor. The sea ice coverage extraction is an outcome of a trained neural network fed with polarimetric features, and borders open water areas.

Our test shows that 88 % of the erroneous drift vectors occurring in open water are filtered out successfully. In the sea ice covered area, we lose 0.4 % of correct drift vectors in consequence of wrong sea ice coverage mapping.

In ongoing work, we validate the drift processor with larger time series and comparison with drift buoys. Moreover the amount of erroneous drift vectors should be further reduced by improvement of the sea ice coverage map and additional quality measures for drift vectors in areas of strongly deformed sea ice.

The processor for sea ice drift estimation is intended to be part of the operational TS-X data processing chain at DLR Ground Station Network sites. Though the chain, derived information products can be provided to navigators and other maritime stakeholders in near real-time (NRT), and assist ship routing in polar waters.

Acknowledgements

This work was supported in part by the funding programme “Maritime Sicherheit – Echtzeitdienste” of the Federal Ministry for Economic Affairs and Energy, Germany. RS-2 products © MDA.

References

[1] C. R. Jackson, J. R. Apel, Synthetic aperture radar: marine user's manual, US Department of Commerce, National Oceanic and Atmospheric Administration, National Environmental Satellite, Data, and Information Serve, Office of Research and Applications, 2004.

[2] IMO, International Code for Ships Operating in Polar Waters (Polar Code). 15 May 2015.

[3] E. De Castro, C. Morandi, Registration of translated and rotated images using finite Fourier transforms, IEEE Transactions on Pattern Analysis & Machine Intelligence 5 (1987): 700-703.

[4] J. Karvonen, Operational SAR-based sea ice drift monitoring over the Baltic Sea, Ocean Science, (2012), 8. Jg., Nr. 4.

[5] T. Hollands. Motion tracking of sea ice with SAR satellite data. Diss. Universität Bremen, 2012.

[6] D. Hamidi, S. Lehner, T. König, A. Pleskachevsky. On the sea ice motion estimation with synthetic aperture radar. In: Proc. 4th TerraSAR-X Meeting (pp. 1-10). 2011.

[7] J. Griebel, W. Dierking, A Method to Improve High-Resolution Sea Ice Drift Retrievals in the Presence of Deformation Zones. Remote Sensing, 9(7), 718 (2017).

[8] R. Ressel, S. Singha, S. Lehner, A. Rösel, G. Spreen, Investigation into different polarimetric features for sea ice classification using X-band Synthetic Aperture Radar. IEEE Journal of Selected Topics in Applied Earth Observations and Remote Sensing, 9 (7), (2016) pp. 3131-3143.

[9] W. David, D. Rod. "The Antarctic Circumnavigation Expedition - an interdisciplinary approach," Book of Abstracts, 2017.

[10] A. Frost, S. Wiehle, S. Singha, D. Krause, Sea ice motion tracking from near real time SAR data acquired during Antarctic Circumnavigation Expedition, IEEE International Geoscience and Remote Sensing Symposium (IGARSS), Valencia, Spain, 2018, 23. - 27. July

[11] H. J. Kramer et al., TerraSAR-X Mission, https://earth.esa.int/web/eoportal/satellite-missions/content/-/article/terrasar-x, (accessed 27.08.2018)

[12] H. J. Kramer et al., RADARSAT-2, https://directory.eoportal.org/web/eoportal/satellite-missions/r/radarsat-2, (accessed 11.09.2018)

[13] Shao, W., Li, X. M., Lehner, S., and Guan, C. 2014. Development of polarization ratio model for sea surface wind field retrieval from TerraSAR-X HH polarization data. International Journal of Remote Sensing, 35(11-12), pp. 4046-4063.

[14] Frost, Anja, Rudolf Ressel, and Susanne Lehner. "Automated iceberg detection using high-resolution X-band SAR images." Canadian Journal of Remote Sensing 42.4 (2016): 354-366.

[15] S. Lehner, T. Krumpen, A. Frost, R. Ressel, T. Busche, E. Schwarz, First tests on near real time ice type classification in Antarctica, IEEE International Geoscience and Remote Sensing Symposium (IGARSS), Québec, Canada, 2014, 13. – 18. July

[16] R. Ressel, A. Frost, S. Lehner, Investigating the potential of different polarimetric features based on dual polarimetric TerraSAR-X data for automated sea ice classification. POLINSAR 2015, Vol. 729. 2015.

[17] R. B. Blackman, J. W. Tukey, The measurement of power spectra from the point of view of communications engineering—Part I. Bell System Technical Journal, (1958) pp. 185-282.

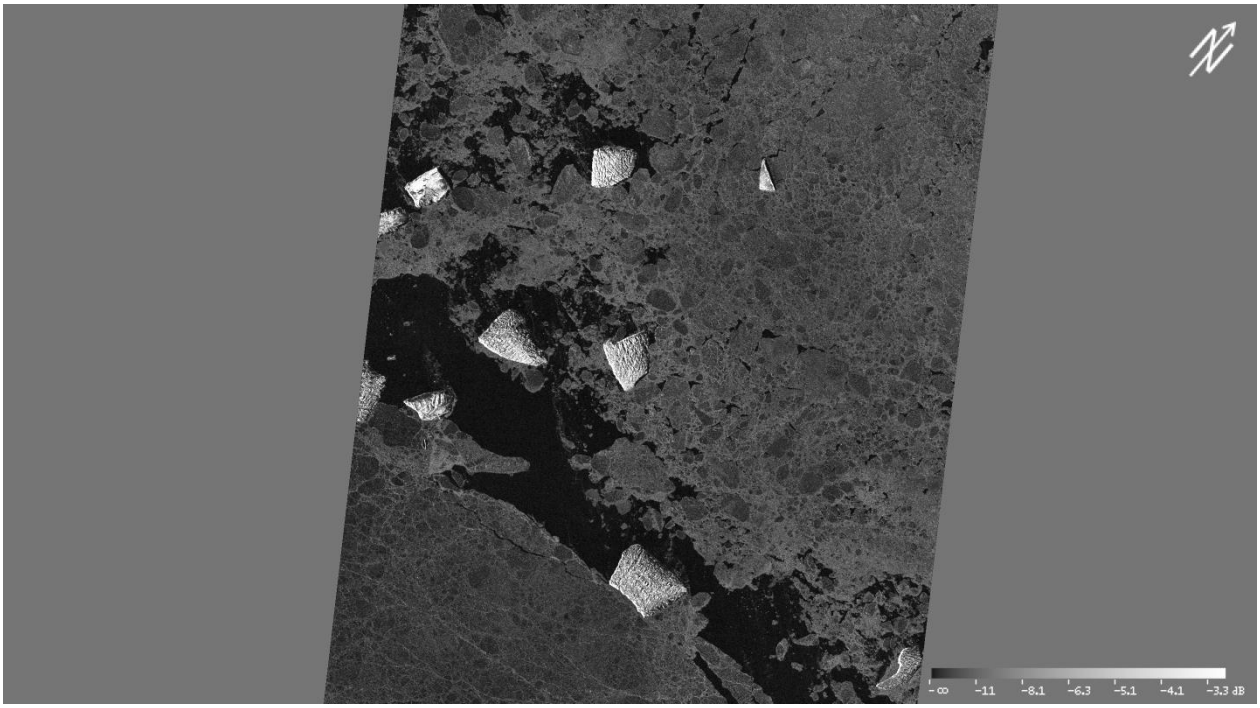

Fig.4. TS-X acquisition taken on 2017/01/30 10:09 UTC over the Southern Ocean close to Cape Denison. The image is calibrated and co-registered to the following RS-2 acquisition shown in Figure 5.

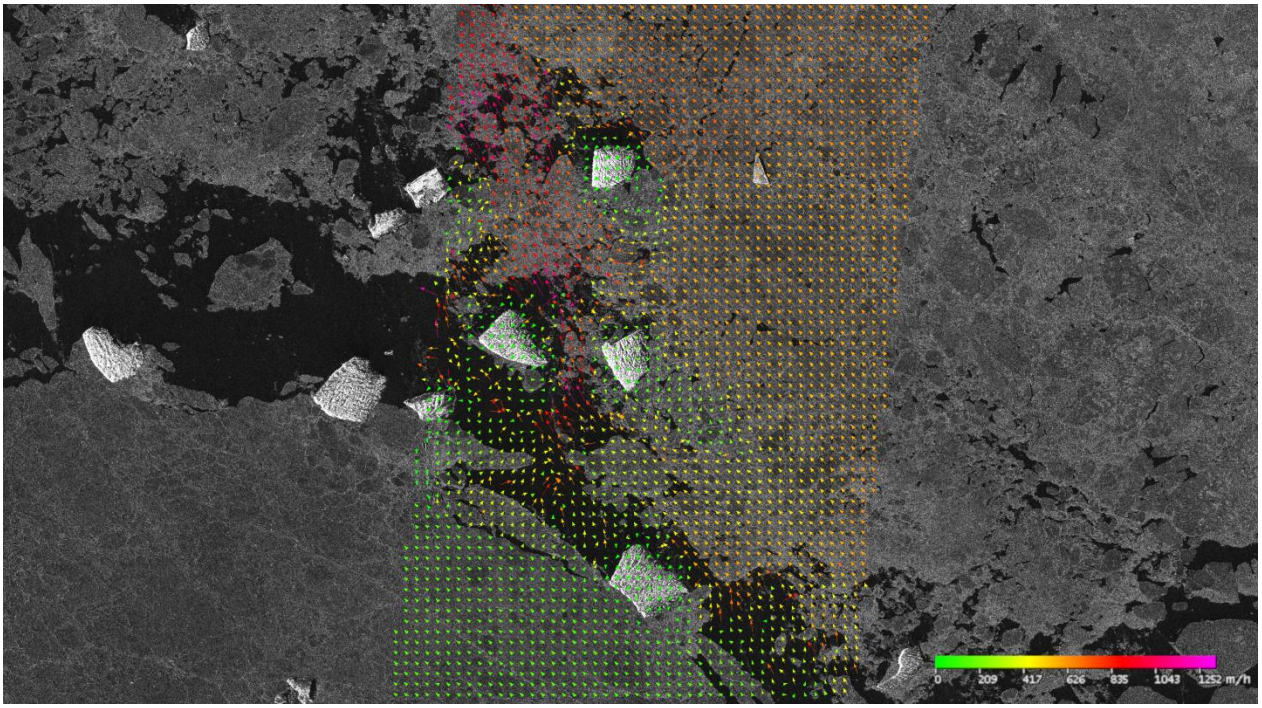

Fig.5. RS-2 acquisition taken on 2017/01/30 10:36 UTC. Color-coded arrows show the sea ice drift field generated from the RS-2 image in the background and the TS-X image in Figure 4.The drift field was generated without sea ice coverage extraction. The resolution of the drift field amounts to 300 m x 300 m.

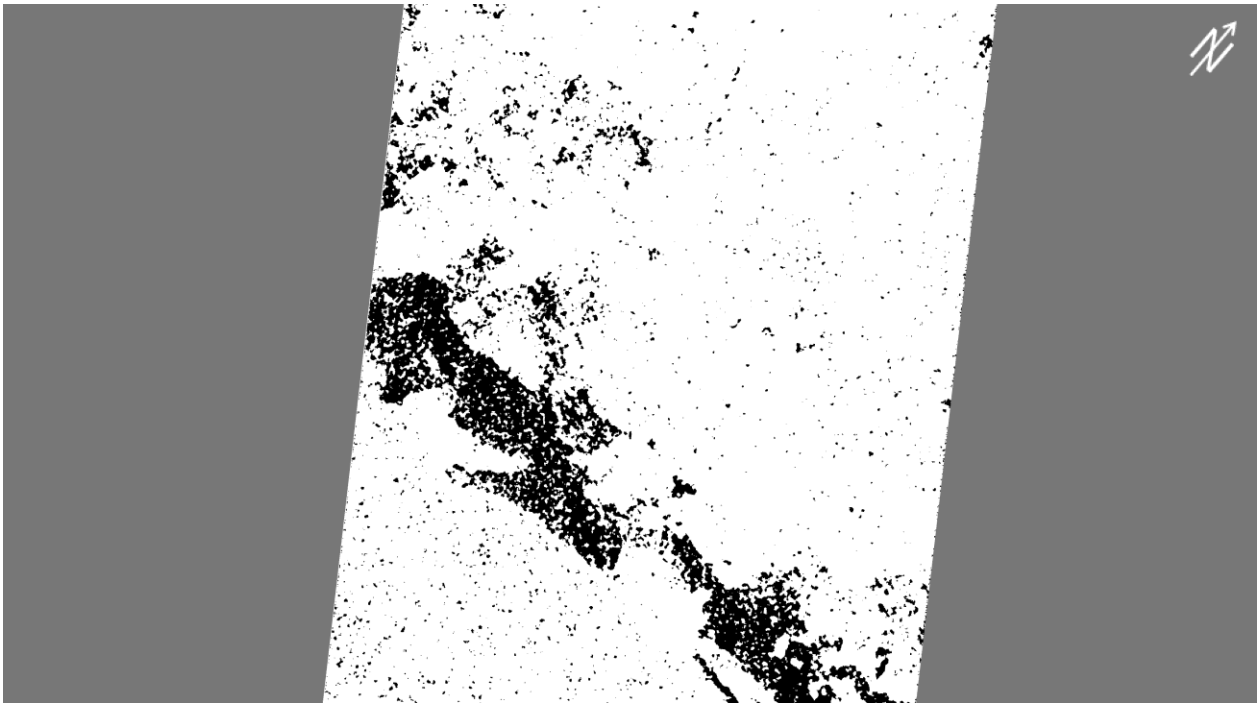

Fig.6. Binary map based on the TS-X acquisition shown in Figure 4. Black pixels correspond to open water. White pixels indicate the presence of sea ice.

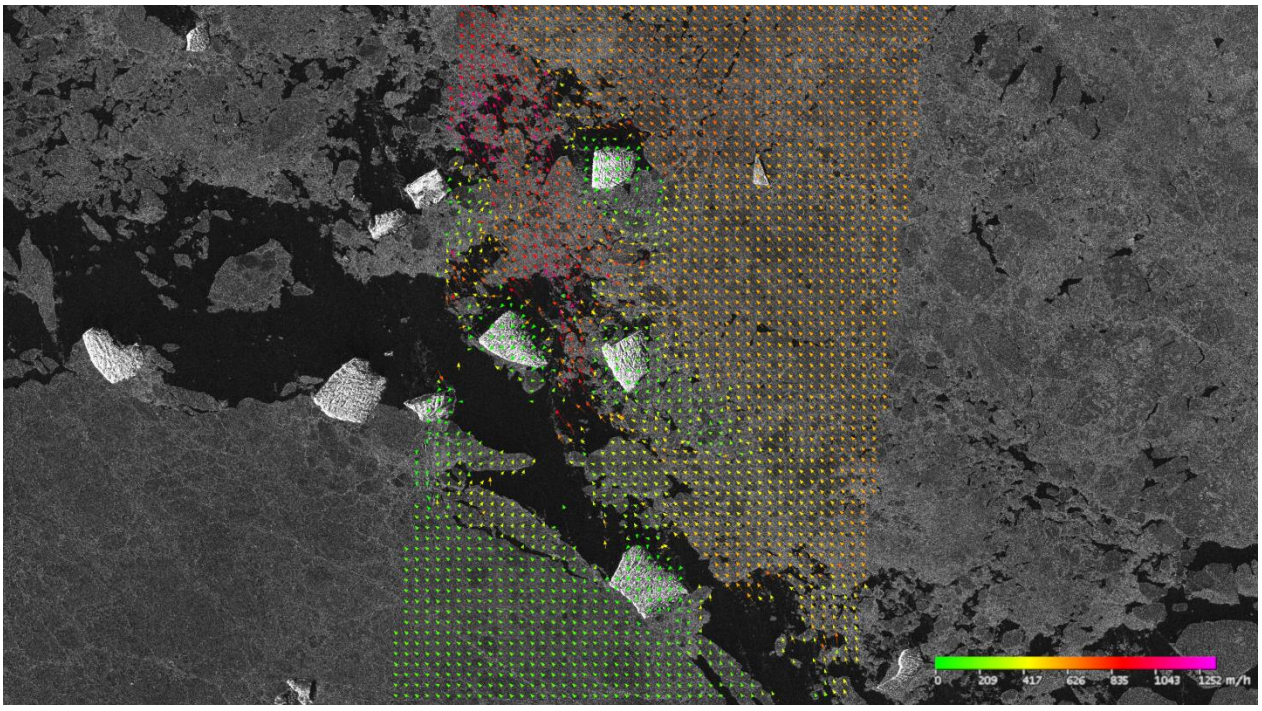

Fig.7. RS-2 acquisition with color-coded drift field considering the sea ice coverage map shown in Figure 6. The drift field was generated with the same parameters as used for generating the drift field shown in Figure 5.

Table 2. Details on the acquisitions shown in Figure 4, 5, and 7

Mission	Mode	Nominal resolution in azimuth	Acquisition date	Acquisition time [UTC]	Incidence angle range	orbit
TS-X	Stripmap Dual Pol	6.6 m	2017/01/30	10:09	42.7°-43.8°	ascending
RS-2	Wide Fine Quad Pol	7.6 m	2017/01/30	10:36	37.8°-40.5°	ascending